*Accelerated Publications*

# Structure of the Ferrous Form of (4-Hydroxyphenyl)pyruvate Dioxygenase from *Streptomyces avermitilis* in Complex with the Therapeutic Herbicide, NTBC[†,‡]

June M. Brownlee,[||] Kayunta Johnson-Winters,[§] David H. T. Harrison,[||] and Graham R. Moran*[,§]

*Department of Biochemistry and Molecular Biology, Rosalind Franklin University of Medicine and Science, 3333 Green Bay Road, North Chicago, Illinois 60064, Department of Chemistry and Biochemistry, University of Wisconsin−Milwaukee, 3210 North Cramer Street, Milwaukee, Wisconsin 53211-3029*

*Received April 6, 2004; Revised Manuscript Received April 19, 2004*

ABSTRACT: Di- and triketone inhibitors of (4-hydroxyphenyl)pyruvate dioxygenase (HPPD) are both effective herbicides and therapeutics. The inhibitory activity is used to halt the production of lipophilic redox cofactors in plants and also in humans to prevent accumulation of toxic metabolic byproducts that arise from specific inborn defects of tyrosine catabolism. The three-dimensional structure of the $Fe^{II}$ form of HPPD from *Streptomyces avermitilis* in complex with the inhibitor 2-[2-nitro-4-(triflouromethyl)benzoyl]-1,3-cyclohexanedione (NTBC) has been determined at a resolution of 2.5 Å. NTBC coordinates to the active site metal ion, located at the bottom of a wide solvent-accessible cavity in the C-terminal domain of the protein. The iron is liganded in a predominantly five-coordinate, distorted square-pyramidal arrangement in which Glu349, His187, and His270 are protein-derived ligands and two other ligands are from the 5′ and 7′ oxygens of NTBC. There is a low-occupancy water molecule in the sixth coordination site in one of the protomers. The distance to His270 is unusually long at 2.5 Å, and its orientation is somewhat distorted from ideal ligand geometry to within 2.8 Å of the inhibitor nitro group. In contrast to the tetrameric quartenary structure observed for HPPD from other bacterial sources, the asymmetric unit is composed of two weakly associated protomers with a buried surface area of 1266 $Å^2$ and a total of 12 hydrogen-bonding and no electrostatic interactions. The overall tertiary structure is similar to that of HPPD from *Pseudomonas fluorescens* (Serre et al., (1999) *Structure 7,* 977−988), although the position of the C-terminal α-helix is dramatically shifted. This C-terminal α-helix provides Phe364, which in combination with Phe336 sandwiches the phenyl ring of the bound NTBC; no other significant hydrogen-bonding or charge-pairing interactions are observed. Moreover, the structure reveals that, with the exception of Val189, NTBC makes contacts to only fully conserved amino acids. The combination of bidentate metal-ion coordination and $\pi$-stacked aromatic rings is suggestive of a binding mode for the substrate and/or a transition state, which may be the origin of the exceedingly high affinity these inhibitors have for HPPD.

With the exception of a number of Gram positive bacteria, (4-hydroxyphenyl)pyruvate dioxygenase (HPPD)[1] is common to all aerobic organisms and catalyzes the second step in the pathway for the catabolism of tyrosine (*1*). HPPD belongs to the α-keto acid-dependent subgroup of ferrous mononuclear non-heme dioxygenases and catalyzes the complex transformation of (4-hydroxyphenyl)pyruvate (HPP) to homogentisate (HG) (Scheme 1).

The primary metabolic function of tyrosine catabolism varies across kingdoms. While the pathway produces energetically exploitable glucogenic and ketogenic products, it has particular importance in plants, where an anabolic branch from homogentisate leads to the production of the essential quinonoid redox cofactors, plastoquinone and tocopherol (*2*) (Scheme 1). Allelopathic triketone alkaloids, such as leptospermone, from myrtaceous plants inhibit HPPD and thus suppress the growth of nearby plants by preventing the formation of these vital quinonoids (*3*, *4*). These observations led to the development of a number of structurally related synthetic inhibitors designed to act as herbicides by specific inhibition of HPPD (*5*−*12*). One of these inhibitors, mesotrione, is the active ingredient in the broad leaf herbicide, Callisto (by Syngenta) (*13*, *14*). Interestingly, another of these inhibitors, 2-[2-nitro-4-(triflouromethyl)benzoyl]-1,3-cyclohexanedi-

[†] This research was supported by the National Institutes of Health Grant DK59551 to G.R.M.

[‡] Atomic coordinates of the HPPD·$Fe^{II}$·NTBC complex have been deposited in the Protein Data Bank (ID code 1T47).

* To whom correspondence should be addressed: Department of Chemistry and Biochemistry, University of Wisconsin−Milwaukee, 3210 N. Cramer St., Milwaukee, Wisconsin 53211-3029. Telephone: 414-229-5031. E-mail: moran@uwm.edu.

[§] University of Wisconsin−Milwaukee.

[||] Rosalind Franklin University of Medicine and Science.

[1] Abreviations: HEPES, *N*-(2-hydroxyethyl)piperizine-*N*′-(2-ethane sulfonic acid); HPPD, (4-hydroxyphenyl)pyruvate dioxygenase; HPP, (4-hydroxyphenyl)pyruvate; NTBC, 2-[2-nitro-4-(triflouromethyl)benzoyl]-1,3-cyclohexanedione; HG, 2,5-dihydroxyphenylacetate; T1Y, hereditary type 1 tyrosinemia; PEG, poly(ethylene glycol); APS, Advanced Photon Source; NCS, noncrystallographic symmetry; MOE, Molecular Operating Environment.

10.1021/bi049317s CCC: $27.50 
Published on Web 05/08/2004

Scheme 1

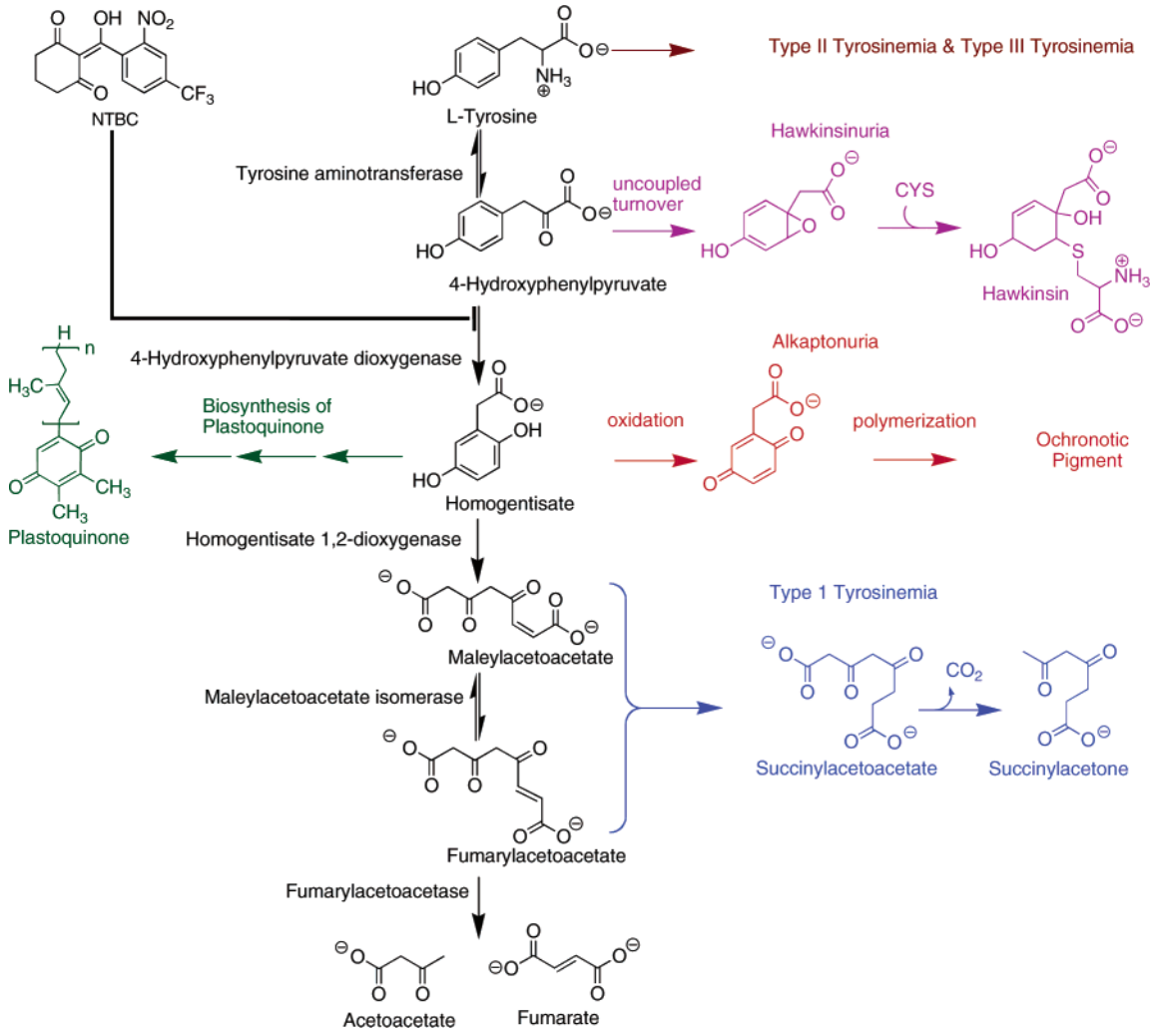


one (NTBC) has been employed therapeutically to treat type 1 tyrosinemia (T1Y) and more recently alkaptonuria (*15*, *16*).

Hereditary T1Y is a fatal autosomal recessive disease that causes hepatic failure, liver cirrhosis, and an early onset of primary liver cancer (*17*). This disease is the result of a defect in the last catalytic step of tyrosine catabolism, the reaction of fumarylacetoacetase. Individuals deficient in this activity accumulate high quantities of hepatotoxic, electrophillic compounds such as succinylacetoacetate and succinylacetone (Scheme 1). Prior to the therapeutic use of HPPD inhibitors, the only treatment for T1Y was liver transplantation. Patients treated with NTBC, administered as Nitisinone (Swedish Orphan Int. AB), now live essentially normal lives, experiencing the relatively mild side effects of elevated blood tyrosine that result in a low incidence of ocular lesions. These side effects, in part, mimic both the symptoms of types II and III tyrosinemia (*15*, *18*).

The first autosomal recessive Mendelian disease trait identified was alkaptonuria and results from a deficiency of active homogentisate 1,2-dioxygenase that leads to the accumulation of the hydroquinone, homogentisate (*19*). This molecule undergoes facile nonenzymatic oxidation and polymerization to yield a highly colored, structurally uncharacterized substance known as the ochronotic pigment. Individuals who have this condition have conspicuous symptoms associated with excretion of the pigment in urine or its accumulation in cartilage and the epidermis. Debilitating chronic symptoms result when accumulation of ochronotic polymers in cartilage and collagenous tissue cause arthritic disability. Recently, NTBC, has been used successfully to treat alkaptonuria patients (*16*).

The ferric form of HPPD from *Pseudomonas fluorescens* in complex with acetate has been previously reported (*20*). This structure revealed the similarity of the fold of HPPD to that of a number of extradiol dioxygenase enzymes having duplicate $\beta$-barrel topology in the N- and C-terminal domains, indicative of gene duplication (*21*, *22*). However, the structure provided no direct information pertaining to key catalytic or inhibitory complexes of the enzyme. Here, we present the first structural characterization of the complex of HPPD in its ferrous form with the paradigm example of the known triketone inhibitors, NTBC. The kinetics of association of NTBC with the ferrous form of HPPD from *Streptomyces avermitilis* was recently demonstrated (*23*). In this earlier investigation, it was definitively shown that the exocyclic enol of the inhibitor (Scheme 1) binds exclusively to the metal ion of the ferrous form of the enzyme. The association occurs in three steps, the last two of which produce charge-transfer absorbances at ~450 nm. The enzyme−inhibitor complex was shown to be irreversibly associated and unreactive toward dioxygen, thus maintaining the $Fe^{II}$ oxidation state. This latter observation provided an

opportunity to crystallize the ferrous enzyme−inhibitor complex under aerobic conditions.

## EXPERIMENTAL PROCEDURES

*Materials.* HPPD from *S. avermitilis* was purified as previously described (*24*) and had a specific activity of 7 $s^{-1}$. NTBC was provided as a gift from Syngenta. Magnesium acetate was purchased from Fisher Scientific. Poly(ethylene glycol) (PEG) 3350 (50%), VDX greased crystallization well plates, 22-mm siliconized cover slides, paratone, and paraffin were each purchased from Hampton Research. Ferrous sulfate was purchased from Sigma−Aldrich.

*Preparation of the HPPD·$Fe^{II}$·NTBC Complex.* The complex of active HPPD with NTBC was made under anaerobic conditions using an adaptation of the method of Kavana and Moran (*23*). A 4.9-mL solution of apo-HPPD (415 $\mu$M) with NTBC (457 $\mu$M) in a 20 mM HEPES buffer at pH 7.0 was made anaerobic in a tonometer at 4 °C by 36 cycles of vacuum and argon, with time for equilibration between each set of three exchanges. Ferrous sulfate (415 $\mu$M final concentration) was then added from a side arm to give a final concentration of 415 $\mu$M HPPD·$Fe^{II}$·NTBC complex, which had a distinctive citrine color because of the metal−ligand charge-transfer absorbance.

*Crystallization of the HPPD·$Fe^{II}$·NTBC Complex.* The initial crystallization conditions for HPPD from *S. avermitilis* were obtained using a PEG ion screen from Hampton Research. The crystals of the complex were clustered needles (individually 50 × 50 × 300 $\mu$M) that appeared within 3−10 days at 4 °C by the vapor diffusion "hanging-drop" method. The composition of the well (500 $\mu$L) was 15% PEG 3350 and 0.4 M magnesium acetate at pH 7.4. The drop (10 $\mu$L) was prepared by mixing equal volumes of the protein−inhibitor complex and the well solution. For cryoprotection, HPPD crystals were washed for a few seconds in the well solution, followed by a brief wash in a 1:3 mixture of paratone and paraffin oil that preceded rapid cooling in liquid nitrogen and storage at 77 °K.

*Structural Determination.* All diffraction data were collected at Advanced Photon Source (APS) (Argonne, IL). A partial data set was initially collected at SER−CAT (22-ID) but radiation damage compromised the diffraction properties of the crystal before data collection could be completed. Subsequently, a complete data set was collected at SBC−CAT (19-ID) using a new crystal. Data were collected at the experimentally determined peak anomalous wavelength (1.7405 Å) at a resolution limit of 2.7 Å. A third crystal provided a complete data set at 2.5 Å using 1.0-Å radiation (19-BM).

Observation of the symmetry and systematic absences showed the crystal to be of the $P2_12_12$ space group with unit-cell dimensions of 81.3 × 162.0 × 56.15 Å. This corresponds to two protomers per unit cell and a 44% solvent content. The data were processed, scaled, and merged with HKL2000 and SCALEPACK (*25*). The data collected at the peak wavelength were analyzed with SOLVE (*26*), thus, locating and refining the positions of two iron atoms of the asymmetric unit and giving a mean figure of merit of 0.31. Modification of the initial phase information including solvent flattening, histogram matching, noncrystallographic symmetry (NCS), and local pattern recognition was performed with RESOLVE and took place iteratively with 50 rounds of the autobuilding/rebuilding function of RESOLVE (*27*). RESOLVE located 560 amino acid residues with side chains belonging to two protomers.

Table 1: Crystal Parameters and Refinement Statistics

| | |
|---|---|
| space group | $P2_12_12$ |
| cell dimensions (Å) | $a = 81.3$ |
| | $b = 162.0$ |
| | $c = 56.2$ |
| $\sigma$ cutoff | 2.0 |
| resolution range (Å) | 30.0−2.5 (2.61−2.50)[a] |
| total no. of reflections | 555 914 |
| no. of unique reflections | 25 574 |
| no. of reflections used in refinement | 23 810 (2451) |
| completeness (%) | 95.5 (75.3) |
| $R_{sym}$ (%) | 5.9 (19.8) |
| $R_{free}$ (%) | 23.8 (36.4) |
| $R$ factor (%) | 17.8 (26.9) |
| Ramachandran most favored/additional (%)[b] | 87.5/12.5 |
| overall mean temperature factor (Å$^2$) | 24.3 |
| rmsd from ideal[c] | |
| bond lengths (Å) | 0.007 |
| bond angles (deg) | 1.5 |

[a] Numbers in parentheses represent the last shell values. [b] Most favored and additional regions as defined by PROCHECK (*41*). [c] Root-mean-square deviations from Engh and Huber ideal values (*42*).

The preliminary protein model determined by RESOLVE clearly demonstrated a similar tertiary structural architecture to the previously reported *P. fluorescens* enzyme. The improved phases were sufficient to calculate an electron density map into which the missing residues could be manually built using the program "O" (*28*) and loosely following the path of the *P. fluorescens* polypeptide. The difference density, after several rounds of building in "O" and refining with XPLOR (*29*), allowed for placement of an NTBC molecule into each active site, liganded to the iron atom. Once the initial model had been built, the data to 2.7 Å were rescaled, averaging the anomalous contributions, and merged with the 2.5-Å data set, using SCALEPACK. This merged data allowed for additional refinement.

*Substrate Modeling.* An in vaccuo model of HPP complexed to $Fe^{II}$ was minimized using the Molecular Operating Environment (MOE) (Chemical Computing Group). The metal ion of this complex was superimposed with the iron atom of the inhibitor complex and rotated so that the position of the phenol ring was aligned with the phenyl ring of NTBC. No further minimization was applied to this model.

## RESULTS

*Stability of the HPPD·$Fe^{II}$·NTBC Complex.* The apparent long-term stability of the complex of HPPD with NTBC in air was previously demonstrated at 4 °C (*23*). To confirm the long-term aerobic stability of this complex, this experiment was repeated at room temperature. The complex was made anaerobically and exposed to atmospheric molecular oxygen, and the spectra were taken over a period of 2.5 days. The holoenzyme in the absence of the inhibitor oxidizes at a rate of 0.01 $s^{-1}$ (*24*); if NTBC were released from the enzyme at an appreciable rate, oxidation of the holoenzyme would be observed as a loss of the metal to ligand charge-transfer absorbance. No significant change in the absorbance at 450 nm was observed during the 2.5 days of observation,

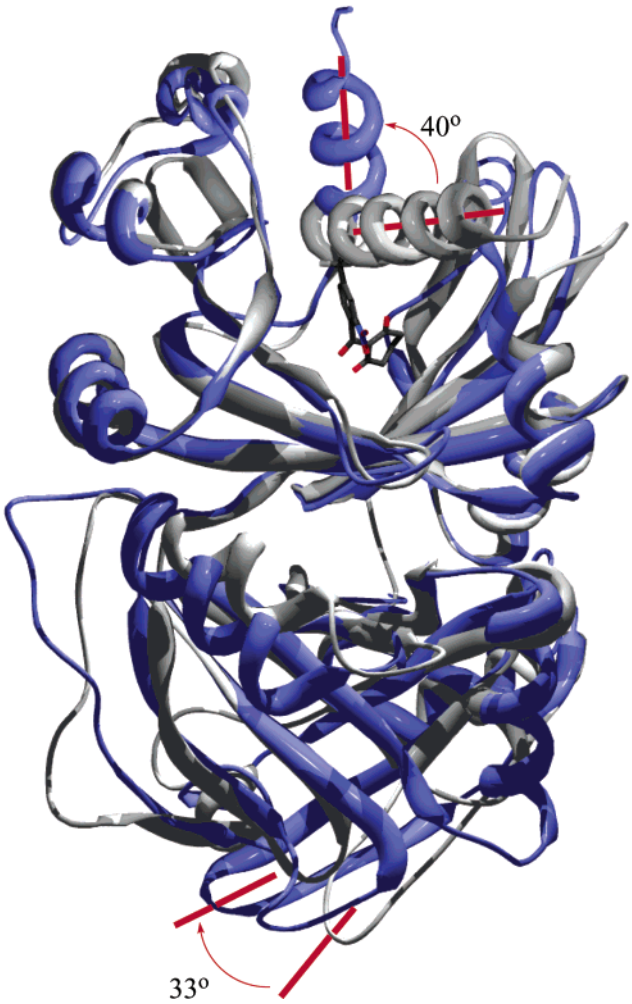


FIGURE 1: Structural overlay of individual protomers from the *S. avermitilis* (blue) to that of *P. fluorescens* (gray). NTBC is depicted in the active site of the *S. avermitilis* structure. The apparent differences in orientation of the C-terminal helix and N-terminal domain $\beta$-strands in the *S. avermitilis* structure are depicted using the axes.

indicating that the complex could be manipulated in the atmosphere without dissociation.

*Overall Structure.* The final model consists of 5838 atoms, comprised of 724 amino acid residues and 274 solvent molecules. In both protomers of the asymmetric unit, the first 15 and the final 4 amino acid residues are disordered and the loop (residues 249−253) and the single helical turn and loop (residues 217−225) show high-temperature factors.

Approximately 3% of the residues were incompletely modeled as alanine or glycine because of the disorder of their side chains; most of these were arginine, lysine, or glutamate or were within high-temperature-factor regions. The final model has a $R$ value of 17.8% ($R_{free}$ = 23.8%). Table 1 lists statistics from the model and the merged data set.

Despite low sequence similarity (~30% identity), the *S. avermitilis* monomer structure is similar with respect to the secondary structure of the *P. fluorescens* enzyme, though the majority of the loops are significantly different. The structure is comprised of two topologically similar $\beta$-barrel domains, inverted and pivoted through 75° with respect to one another, suggesting gene duplication. The root-mean-square (RMS) deviation of the $\beta$-barrel α-carbon positions compared with the *P. fluorescens* structure is 1.3 Å. There are two significant differences in the placement of the secondary structure elements relative to the *P. fluorescens* enzyme structure. The first is the $\beta$-strands and intervening turn 130−143 (residues 106−116 in *P. fluorescens*) that pack differently because of the increased length of the $\beta$ structure and the position of the turn, which differs by 7 Å between structures. The second difference is that the C-terminal α-helix is displaced out of the active site by ~40° (Figure 1).

The two protomers in the asymmetric unit form an interface that buries 1266 Å$^2$ (8.3%) of the monomer solvent-accessible surface. The residues in this interface are 44% polar with 12 potential hydrogen bonds and no salt bridges that span the two protomers. Although the interface of the *S. avermitilis* enzyme shares a significant degree of sequence identity (80%) among hydrogen-bonding residues with the rat and human enzymes, the fact that this protein−protein interface is not seen in the tetrameric *P. fluorescens* structure combined with its hydrophilic nature suggests that the interface is unlikely to be important to catalysis. In vivo, this interface is likely to represent the site of either dimerization or some other protein−protein interaction (*30*).

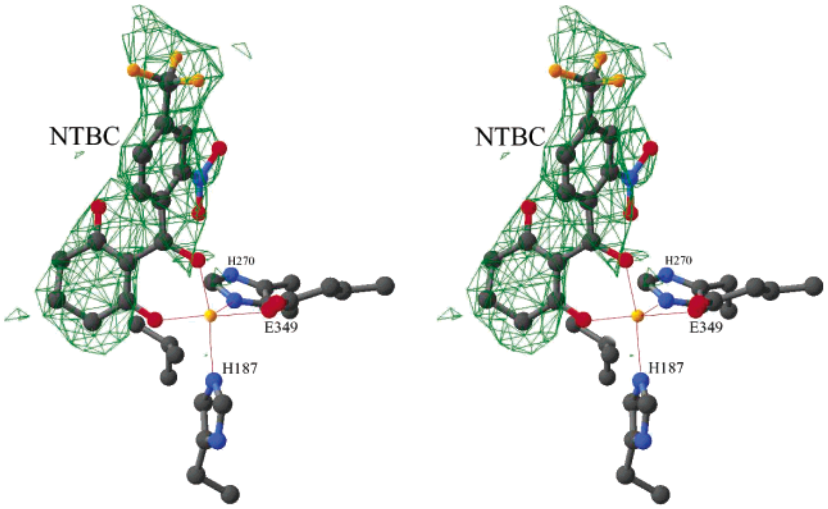


FIGURE 2: Stereoview of an unbiased difference electron density map using the Fourier coefficients $F_o - F_c$ (calculated early during the structure refinement just prior to adding the NTBC atoms to the model) observed near the NTBC superimposed on the final atomic model of the metal-ion coordination sphere. The electron density suggests an unambiguous placement of the NTBC model.

A

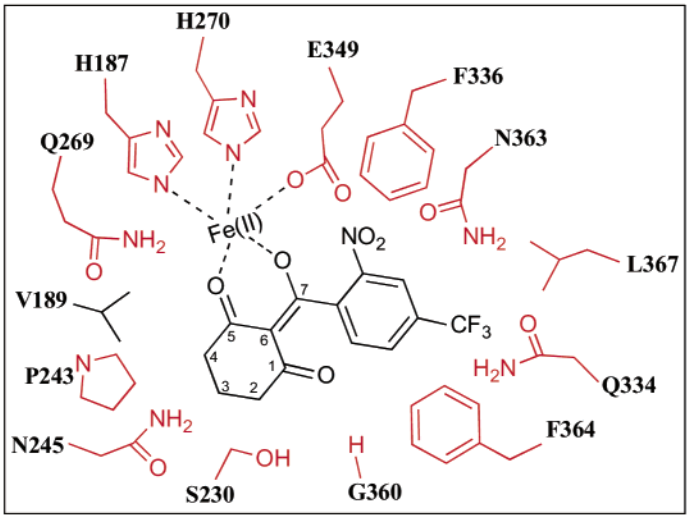


B

```
HUMAN             1          TTYS-------------------DKGAKPERGRFLHFHSVTFWVGNAKQAASFYCSKMGFEPLAYRGLETG  52
PIG               1          TSYS-------------------DKGEKPERGRFLHFHSVTFWVGNAKQAASYYCSKIGFEPLAYKGLETG  52
BARLEY            1     MPPTPTTPAATGAAAAVTPEHARPHRMVRFNPRSDRFHTLSFHHVEFWCADAASAAGRFAFALGAPLAARSDLSTG  76
CARROT            1 MGKKQSEAEILSSNSSNTSPATFKLVGFNNFVRANPKSDHFAVKRFHHIEFWCGDATNTSRRFSWGLGMPLVAKSDLSTG  80
P fluorescens     1                                ADLYENPMGLMGFEFIEFASPTPGTLEPIFEIMGFTKVATHR-----  42
S. avermilitis    1       MTQTTHHTP-----------------DTARQADPFPVKGMDAVVFAVGNAKQAAHYYSTAFGMQLVAYSGPENG  57

HUMAN            53 SREVVSHVIKQGKIVFVLSSALN------------PWNKEMGDH--LVKHGDGVKDIAFEVEDCDYIVQKARERGAKIMR 118
PIG              53 SREVVSHVVKQDKIVFVFSSALN------------PWNKEMGDH--LVKHGDGVKDIAFEVEDCDYIVQKARERGAIIVR 118
BARLEY           77 NSAHASQLLRSGSLAFLFTAPYANGCDAAT--ASLPSFSADAARRFSADHGIAVRSVALRVADAAEAFRASRRRGARPAF 154
CARROT           81 NSVHASYLVRSANLSFVFTAPYSPSTTTSSGSAAIPSFSASGFHSFAAKHGLAVRAIALEVADVAAAFEASVARGARPAS 160
P fluorescens    43 SKN--VHLYRQGEINLILNNEPN------------SIASYFAAE-----HGPSVCGMAFRVKDSQKAYNRALELGAQPIH 103
S avermilitis    58 SRETASYVLTNGSARFVLTSVIKP---------ATPWGHFLADH--VAEHGDGVVDLAIEVPDARAAHAYAIEHGARSVA 126

HUMAN           119 EPWVEQDKFGKVKFAVLQTYGDTTHTLVEKMN-YIGQFLPG-YEAPAFMDPLLPKLPKCSLEMIDHIVGNQPDQEMVSAS 196
PIG             119 EEVCCAADVRGHHTPLDRARQVWEGTLVEKMT-FCLDSRPQ-PSQTLLHRLLLSKLPKCGLEIIDHIVGNQPDQEMESAS 196
BARLEY          155 APVDLGR---GFAFAEVELYGDVVLRFVSHPDGTDVPFLPGF--EGVTN----PDAVDYGLTRFDHVVGNVP--ELAPAA 223
CARROT          161 APVELDD---QAWLAEVELYGDVVLRFVSFGR-EEGLFLPGF--EAVEGTASFPD-LDYGIRRLDHAVGNVT--ELGPVV 231
P fluorescens   104 IDTGPME----LNLPAIKGIGGAPLYLIDRFG--EGSSIYD--IDFVYLEGVERNPVGAGLKVIDHLTHNVYRGRMVYWA 175
S avermilitis   127 EPYELKDEHGTVVLAAIATYGKTRHTLVDRTG-YDGPYLPG----YVAAAPIVEPPAHRTFQAIDHCVGNVELGRMNEWV 201

HUMAN           197 EWYLKNLQFHRFWSVDDTQVHTEYSSLRSIVVANYEESIKMPINEPAPGKKK-SQIQEYVDYNGGAGVQHIALKTEDIIT 275
PIG             197 QWYMRNLQFHRFWSVDDTQIHTEYSALRSVVMANYEESIKMPINEPAPGKKK-SQIQEYVDYNGGAGVQHIALKTEDIIT 275
BARLEY          224 AYIAGFTGFHEFAEFTAEDVGTTESGLNSVVLANNSEGVLLPLNEPVHGTKRRSQIQTFLEHHGGPGVQHIAVASSDVLR 303
CARROT          232 EYIKGFTGFHEFAEFTAEDVGTLESGLNSVVLANNEEMVLLPLNEPVYGTKRKSQIQTYLEHNEGAGVQHLALVSEDIFR 311
P fluorescens   176 NFYEKLFNFREARYF---DIKGEYTGLTSKAMSAPDGMIRIPLNEESSKGAG--QIEEFLMQFNGEGIQHVAFLTDDLVK 250
S avermilitis   202 GFYNKVMGFTNMKEFVGDDIATEYSALMSKVVADGTLKVKFPINEPALAKKK-SQIDEYLEFYGGAGVQHIALNTGDIVE 280

HUMAN           276 AIRHLRER----GLEFLSVP-STYYKQLREKLKTAKIKVKENIDALEELKILVDYD----EKGYLLQIFTKPVQDRPTLF 346
PIG             276 AIRSLRER----GVEFLAVP-FTYYKQLQEKLKSAKIRVKESIDVLEELKILVDYD----EKGYLLQIFTKPMQDRPTVF 346
BARLEY          304 TLRKMRARSAMGGFDFLPPPLPKYYEGVRRLAG--DVLSEAQIKECQELGVLVDRD----DQGVLLQIFTKPVGDRPTLF 377
CARROT          312 TLREMRKRSCLGGFEFMPSPPPTYYKNLKNRVG--DVLSDEQIKECEDLGILVDRD----DQGTLLQIFTKPVGDRPTLF 385
P fluorescens   251 TWDALKKI----GMRFMTAPPDTYYEMLEGRLP----DHGEPVDQLQARGILLDGSSVEGDKRLLLQIFSETLMG--PVF 320
S avermilitis   281 TVRTMRAA----GVQFLDTP-DSYYDTLGEWVG----DTRVPVDTLRELKILADRD----EDGYLLQIFTKPVQDRPTVF 347

HUMAN           347 LEVIQRH---------------NHQGFGAGNFNSLFKAFEEEQNLRGNLTNMETNGVVPGM 392   46%
PIG             347 LEVIQRN---------------NHQGFGAGNFNSLFKAFEEEQELRGNLTDTDPNGVPFRL 392   41%
BARLEY          378 LEMIQRIGCMEKDERGEEYQKGGCGGFGKGNFSELFKSIEDYEKSLEAKQSAAVQGS     434   36%
CARROT          386 IEIIQRVGCMLKDDAGQMYQKGGCGGFGKGNFSELFKSIEEYEKTLEAKQITGSAAA     442   38%
P fluorescens   321 FEFIQRK---------------GDDGFGEGNFKALFESIERDQVRRGVLATD          357   31%
S avermilitis   348 FEIIERH---------------GSMGFGKGNFKALFEAIEREQEKRGNL            381   51 Identities
```

FIGURE 3: (A) Active site residues in van der Waals contact (<4 Å) with NTBC. (B) Sequence alignment of the *S. avermitilis* primary structure compared to that of *P. fluorescens*, carrot, barley, pig, and human. Amino acids depicted in black are not conserved, while those in red are conserved and those in blue show similarity in all sequences. Sequences underlined are within 10 Å of the active-site metal ion. The identity is indicated at the C terminus as a percentage of the *S. avermitilis* sequence.

*Association of NTBC.* Figure 2 depicts the complex of NTBC with the active site metal ion of HPPD. The inhibitor is observed to form a bidentate association with the active-site metal ion via its 5′ and 7′ oxygens forming a predominantly five-coordinate, distorted square-pyramidal complex. Only one of the two protomers has evidence of a low-occupancy/high-temperature-factor water ligand in the sixth-coordinate position. The conformation of NTBC has the two rings oriented ~80° with respect to one another. The 5′ and 7′ oxygens that ligand the metal are best-fit to the electron density when they are out of the plane by ~14°, suggesting that the planar exocyclic enol is not dominant at equilibrium on the surface of the enzyme. However, the resolution of the available data does not permit definitive tautomeric assignment of the inhibitor. The 1′ oxygen makes no contact with active-site amino acids, consistent with the strong inhibition observed with structurally related diketone inhibitors (*8*, *11*, *31*). The aromatic ring of NTBC is sandwiched

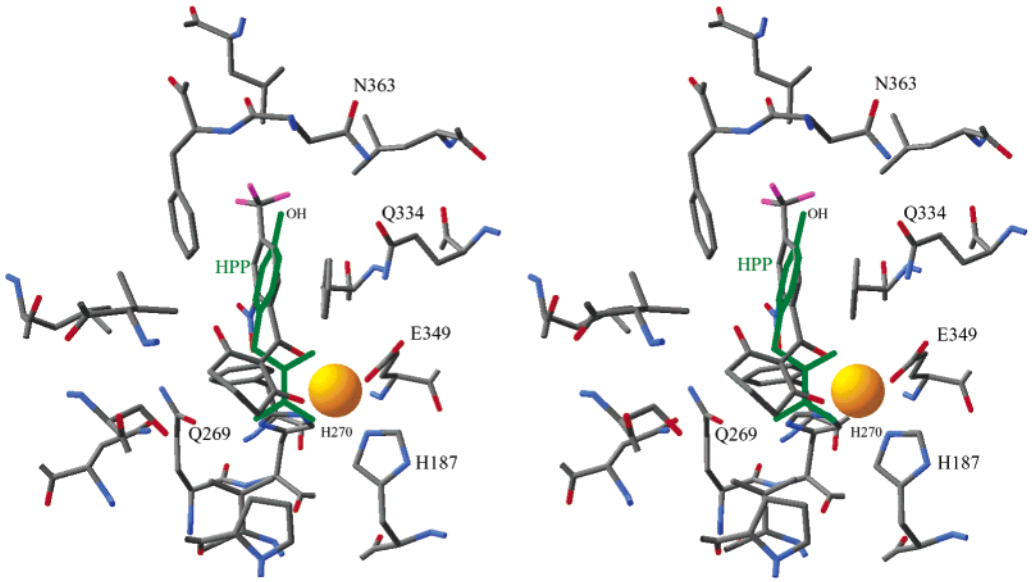


FIGURE 4: Stereoview of all amino acid residues within 5 Å of NTBC (omitting the residues Phe358, Gly359, Val360, and Asn245 for image clarity). The substrate of the enzyme, HPP, has been modeled into the space occupied by NTBC (shown in green).

Table 2: $Fe^{II}$−Ligand Distances (Å)[a]

| | | | |
|---|---|---|---|
| O (Glu349) | 2.2 | O (NTBC 7′) | 2.0 |
| N (His270) | 2.6 | O (NTBC 5′) | 2.0 |
| N (His187) | 2.3 | O ($H_2O$)[b] | 2.4 |

[a] Average distance observed from both protomers. [b] High-temperature factor and/or low occupancy in one of the two protomers of the asymmetric unit.

between the phenyl rings of conserved phenylalanines 336 and 364 (Figures 3 and 4). The trifluoromethyl substituent makes only contact interaction with surrounding amino acids, the closest of which are with the side chains of Asn363 and Leu367. One of the nitro substituent oxygens is 2.8-Å from the epsilon carbon of His270 as modeled (one of the facial triad of residues that ligands the active-site metal ion). The orientation and proximity of the nitro group with respect to His270 suggests that rotation of the imidazole ring would permit a direct hydrogen-bonding interaction. In addition, His270 is also the most distant metal-ion ligand at 2.6 Å from the metal atom (Table 2).

*Modeling the Substrate-Binding Mode.* Figure 4 depicts a proposed conformation and binding orientation for HPP based on both the previously observed bidentate association of α-ketoglutarate in a number of α-keto acid-dependent enzymes (*32*−*34*) and the recent spectroscopic description of the HPPD substrate complex (*35*). Additionally, the phenyl ring of the substrate was placed similarly to that of the inhibitor.

## DISCUSSION

The capacity to synthesize specific inhibitors of HPPD gave an evolutionary advantage to a number of plants and lichens as a means of suppressing the growth of competing nearby plants. This inhibition prevented the synthesis of homogentisate from HPP in the tyrosine catabolism pathway, thereby halting the production of essential quinonoid redox cofactors used in photosynthesis (Scheme 1). Structural elucidation of these inhibitory alkaloids has led directly to the development of similar molecules for use as herbicides. The ubiquitous nature of this pathway in aerobic metabolism, however, has meant that specific inhibition of HPPD has also been of significant therapeutic benefit to mankind, providing a viable means of eliminating the symptoms of debilitating and life-threatening inherited illnesses that arise from defects in tyrosine catabolism.

Despite the importance of HPPD inhibition, a structural depiction of the mode of this inhibition has hitherto not been reported. The only available structural data was the crystal structure of HPPD from *P. fluorescens*, solved in the ferric form of the enzyme and with acetate-liganded monodentate to the metal ion to give a distorted tetragonal geometry (*20*). In a recent kinetic characterization of the association of the inhibitor NTBC with HPPD from *S. avermitilis*, no interaction of the inhibitor with the ferric form was observed, whereas complexation of the inhibitor with the ferrous form of the enzyme was irreversible. Moreover, the ferrous enzyme−inhibitor complex was maintained in part by a complete suppression of dioxygen reactivity (*23*). The latter phenomenon has provided an opportunity to crystallize and solve the structure of the inhibitory complex of this form of HPPD with NTBC bound in the inhibitory site.

A lack of oxygen reactivity has been predicted for the complex of NTBC with HPPD; it was proposed that the inhibitor would physically block dioxygen access to the metal center (*36*). However, the active-site metal ion in complex with the inhibitor is observed to be predominantly five-coordinate and the conformation of the inhibitor is such that it does not prevent access to the metal ion. We can conclude that the observed suppression of dioxygen reactivity in the inhibitor complex is not controlled sterically by the inhibitor (Figure 2).

In Modeling HPP, it was not possible to simultaneously coordinate the iron and align the substrate to stack as well as the inhibitor against the two-conserved phenylalanine residues, suggesting that the protein may adopt more than one conformation during the catalytic cycle (Figure 4). Modeling the substrate into the NTBC volume indicates that a number of conserved amide residues are available to form hydrogen bonds with substrate oxygens in such an orienta-

tion. In this inhibited structure, Asn363 forms a hydrogen bond with Gln334, and either of them would be positioned to hydrogen-bond with the HPP phenol hydroxyl. Gln334 is within hydrogen-bonding distance to Glu349 that ligands the metal ion. These residues (363, 334, and 349) may thus provide a means to sense the presence of the substrate 4-hydroxyl and thereby explain the complete lack of catalytic activity observed with phenylpyruvate for HPPD from *S. avermitilis* (*24*). At the pyruvate substituent, the conserved residues Asn245 and Gln269 are oriented in the current structure to interact with the carboxylate, although a substantial conformational change would need to occur to bring these residues within hydrogen-bonding distance of HPP.

In the structure presented, NTBC is observed to localize adjacent to the metal ion by coordination from the 5′ and 7′ oxygens. This is one of the two primary binding interactions observed in the complex. The other is the placement of the NTBC aromatic ring between conserved phenylalanines 336 and 364. Unexpectedly, no other specific hydrogen-bonding or charge-pairing interactions are observed, and van der Waals contacts are made primarily with fully conserved amino acid side chains. Moreover, the internal active-site surface of HPPD is highly conserved, suggesting that the selectivity observed with a number of known HPPD inhibitors among different plant and animal species is more reliant on delivery and/or metabolic processing than it is on the structural origin of the enzyme (*13*, *14*, *37*, *38*). This assertion is consistent with what is observed for the naturally occurring HPPD inhibitor, usnic acid, where both the (+) and (−) enantiomers are observed to inhibit in vitro, but only the (−) form is active on the whole plant (*39*).

One potentially significant difference in the fold of the peptide of this structure compared with that of the *P. fluorescens* enzyme is the position of the C-terminal α-helix. This helix is angled 40° into the solvent with respect to the original HPPD structure (Figure 1). This difference may be evidence of structural dynamics in ligand binding because the C-terminal α-helix provides Phe364, which in combination with Phe336 sandwiches the phenyl ring of the bound NTBC. The placement of the phenyl ring of the inhibitor may approximate the position of the ring of the substrate. If this were the case, it would be reasonable to surmise that the inhibitor association mimics a specific catalytic step and that this is the origin of the high affinity that these inhibitors have for the enzyme. Earlier observations of slow, tight association are consistent with the association of a transition-state-like molecule (*23*, *40*).

## CONCLUDING REMARKS

Specific inhibition of HPPD has been of significant benefit to mankind. HPPD inhibitors are both powerful selective herbicides and therapeutics that can offer complete cessation of the symptoms of lethal and/or incapacitating diseases. The description of the ferrous form of HPPD in complex with the paradigm example of such inhibitors, NTBC, is a significant advance in understanding the inhibitory mechanism. In this regard, what is suggested from this structure is that the interaction of triketone inhibitors with HPPD is topologically conserved and species selectivity must therefore arise from differences in bioavailability.

## ACKNOWLEDGMENT

Use of the Argonne National Laboratory Structural Biology Center beamlines at the Advanced Photon Source was supported by the U.S. Department of Energy, Office of Energy Research, under contract no. W-31-109-ENG-38.

## REFERENCES

1. Gunsior, M., Ravel, J., Challis, G. L., and Townsend, C. A. (2004) Engineering *p*-hydroxyphenylpyruvate dioxygenase to a *p*-hydroxymandelate synthase and evidence for the proposed benzene oxide intermediate in homogentisate formation, *Biochemistry 43*, 663−674.
2. Goodwin, T. W., and Mercer, E. I. (1983) *Introduction to Plant Biochemistry*, 2nd ed., Pergamon Press, Sydney, Australia.
3. Hellyer, R. (1968) The occurrence of β-triketones in the steam-volatile oils of some myrtaceous australian plants, *Austr. J. Chem. 21*, 2825−2828.
4. Schulz, A., Ort, O., Beyer, P., and Kleinig, H. (1993) SC-0051, a 2-benzoyl-cyclohexane-1,3-dione bleaching herbicide, is a potent inhibitor of the enzyme *p*-hydroxyphenylpyruvate dioxygenase, *FEBS Lett. 318*, 162−166.
5. Secor, J. (1994) Inhibition of Barnyardgrass 4-Hydroxyphenylpyruvate Dioxygenase by Sulcotrione, *Plant Physiol. 106*, 1429−1433.
6. Lin, S., and Yang, D. (1999) Inhibition of 4-hydroxyphenylpyruvate dioxygenase by sethoxydim, a potent inhibitor of acetyl-coenzyme A carboxylase, *Bioorg. Med. Chem. Lett. 9*, 551−554.
7. Ling, T. S., Shiu, S., and Yang, D. Y. (1999) Design and synthesis of 3-fluoro-2-oxo-3-phenylpropionic acid derivatives as potent inhibitors of 4-hydroxyphenylpyruvate dioxygenase from pig liver, *Bioorg. Med. Chem. 7*, 1459−1465.
8. Garcia, I., Job, D., and Matringe, M. (2000) Inhibition of *p*-hydroxyphenylpyruvate dioxygenase by the diketonitrile of isoxaflutole: A case of half-site reactivity, *Biochemistry 39*, 7501−7507.
9. Lin, S. W., Lin, Y. L., Lin, T. C., and Yang, D. Y. (2000) Discovery of a potent, nontriketone type inhibitor of 4-hydroxyphenylpyruvate dioxygenase, *Bioorg. Med. Chem. Lett. 10*, 1297−1298.
10. Lin, Y. L., Wu, C. S., Lin, S. W., and Yang, D. Y. (2000) SAR studies of 2-*o*-substituted-benzoyl- and 2-alkanoyl-cyclohexane-1,3-diones as inhibitors of 4-hydroxyphenylpyruvate dioxygenase, *Bioorg. Med. Chem. Lett. 10*, 843−845.
11. Huang, M., Yang, D. Y., Shang, Z., Zou, J., and Yu, Q. (2002) 3D-QSAR studies on 4-hydroxyphenylpyruvate dioxygenase inhibitors by comparative molecular field analysis (CoMFA), *Bioorg. Med. Chem. Lett. 12*, 2271−2275.
12. Huang, J. L., Liu, H. G., and Yang, D. Y. (2003) Acylcyclohexanedione derivatives as potential in vivo sequential inhibitors of 4-hydroxyphenylpyruvate dioxygenase and GA(20) 3-β-hydroxylase, *Bioorg. Med. Chem. Lett. 13*, 927−930.
13. Mitchell, G., Bartlett, D. W., Fraser, T. E., Hawkes, T. R., Holt, D. C., Townson, J. K., and Wichert, R. A. (2001) Mesotrione: A new selective herbicide for use in maize, *Pest Manage. Sci. 57*, 120−128.
14. Sutton, P., Richards, C., Buren, L., and Glasgow, L. (2002) Activity of mesotrione on resistant weeds in maize, *Pest Manage. Sci. 58*, 981−984.
15. Lindstedt, S., Holme, E., Lock, E. A., Hjalmarson, O., and Strandvik, B. (1992) Treatment of hereditary tyrosinaemia type I by inhibition of 4-hydroxyphenylpyruvate dioxygenase, *Lancet 340*, 813−817.
16. Phornphutkul, C., Introne, W. J., Perry, M. B., Bernardini, I., Murphey, M. D., Fitzpatrick, D. L., Anderson, P. D., Huizing, M., Anikster, Y., Gerber, L. H., and Gahl, W. A. (2002) Natural history of alkaptonuria, *N. Engl. J. Med. 347*, 2111−2121.
17. Holme, E., and Lindstedt, S. (1998) Tyrosinaemia type I and NTBC (2-(2-nitro-4-trifluoromethylbenzoyl)-1,3-cyclohexanedione), *J. Inherited Metab. Dis. 21*, 507−517.
18. Ahmad, S., Teckman, J. H., and Lueder, G. T. (2002) Corneal opacities associated with NTBC treatment, *Am. J. Ophthalmol. 134*, 266−268.
19. Garrod, E. A. (1902) The incidence of alkaptonuria: A study in clinical individuality, *Lancet 2*, 1616−1620.
20. Serre, L., Sailland, A., Sy, D., Boudec, P., Rolland, A., Pebay-Peyroula, E., and Cohen-Addad, C. (1999) Crystal structure of

*Pseudomonas fluorescens* 4-hydroxyphenylpyruvate dioxygenase: An enzyme involved in the tyrosine degradation pathway, *Structure 7*, 977−988.
21. Han, S., Eltis, L. D., Timmis, K. N., Muchmore, S. W., and Bolin, J. T. (1995) Crystal structure of the biphenyl-cleaving extradiol dioxygenase from a PCB-degrading pseudomonad, *Science 270*, 976−980.
22. Senda, T., Sugiyama, K., Narita, H., Yamamoto, T., Kimbara, K., Fukuda, M., Sato, M., Yano, K., and Mitsui, Y. (1996) Three-dimensional structures of free form and two substrate complexes of an extradiol ring-cleavage type dioxygenase, the BphC enzyme from *Pseudomonas* sp. strain KKS102, *J. Mol. Biol. 255*, 735−752.
23. Kavana, M., and Moran, G. R. (2003) Interaction of (4-hydroxyphenyl)pyruvate dioxygenase with the specific inhibitor 2-[2-nitro-4-(trifluoromethyl)benzoyl]-1,3-cyclohexanedione, *Biochemistry 42*, 10238−10245.
24. Johnson-Winters, K., Purpero, V. M., Kavana, M., Nelson, T., and Moran, G. R. (2003) (4-Hydroxyphenyl)pyruvate dioxygenase from *Streptomyces avermitilis*: The basis for ordered substrate addition, *Biochemistry 42*, 2072−2080.
25. Otwinowski, Z., and Minor, W. (1997) Processing of X-ray diffraction data collected in oscillation mode. *Methods Enzymol. 276*, 307−325.
26. Terwilliger, T. C. (1997) Multiwavelength anomalous diffraction phasing of macromolecular structures: Analysis of MAD data as single isomorphous replacement with anomalous scattering data using the MADMRG Program, *Methods Enzymol. 276*, 530−537.
27. Terwilliger, T. (2004) SOLVE and RESOLVE: Automated structure solution, density modification, and model building, *J. Synchrotron Radiat. 11*, 49−52.
28. Jones, T. A., Zou, J. Y., Cowan, S. W., and Kjeldgaard, M. (1991) Improved methods for building protein models in electron density maps and the location of errors in these models, *Acta Crystallogr., Sect. A 47* (Part 2), 110−119.
29. Brunger, A. T. (1992) *XPLOR*, Yale University Press, New Haven, CT.
30. Jones, S., and Thornton, J. M. (1996) Principles of protein−protein interactions, *Proc. Natl. Acad. Sci. U.S.A. 93*, 13−20.
31. Wu, C. S., Huang, J. L., Sun, Y. S., and Yang, D. Y. (2002) Mode of action of 4-hydroxyphenylpyruvate dioxygenase inhibition by triketone-type inhibitors, *J. Med. Chem. 45*, 2222−2228.
32. Elkins, J. M., Ryle, M. J., Clifton, I. J., Dunning Hotopp, J. C., Lloyd, J. S., Burzlaff, N. I., Baldwin, J. E., Hausinger, R. P., and Roach, P. L. (2002) X-ray crystal structure of *Escherichia coli* taurine/α-ketoglutarate dioxygenase complexed to ferrous iron and substrates, *Biochemistry 41*, 5185−5192.
33. Zhang, Z., Ren, J., Harlos, K., McKinnon, C. H., Clifton, I. J., and Schofield, C. J. (2002) Crystal structure of a clavaminate synthase-Fe(II)-2-oxoglutarate−substrate-NO complex: Evidence for metal centred rearrangements, *FEBS Lett. 517*, 7−12.
34. Valegard, K., van Scheltinga, A. C., Lloyd, M. D., Hara, T., Ramaswamy, S., Perrakis, A., Thompson, A., Lee, H. J., Baldwin, J. E., Schofield, C. J., Hajdu, J., and Andersson, I. (1998) Structure of a cephalosporin synthase, *Nature 394*, 805−809.
35. Neidig, M. L., Kavana, M., Moran, G. R., and Solomon, E. I. (2004) CD and MCD Studies of the non-heme ferrous active site in (4-hydroxyphenyl)pyruvate dioxygenase: Correlation between oxygen activation in the extradiol and α-KG dependent dioxygenases, *J. Am. Chem. Soc. 126*, 4486−4487.
36. Hanauske-Abel, H. M., Popowicz, A., Remotti, H., Newfield, R. S., and Levy, J. (2002) Tyrosinemia I, a model for human diseases mediated by 2-oxoacid-utilizing dioxygenases: Hepatotoxin suppression by NTBC does not normalize hepatic collagen metabolism, *J. Pediatr. Gastroenterol. Nutr. 35*, 73−78.
37. Dyson, J. S., Beulke, S., Brown, C. D., and Lane, M. C. (2002) Adsorption and degradation of the weak acid mesotrione in soil and environmental fate implications, *J. Environ. Qual. 31*, 613−618.
38. Hall, M. G., Wilks, M. F., Provan, W. M., Eksborg, S., and Lumholtz, B. (2001) Pharmacokinetics and pharmacodynamics of NTBC (2-(2-nitro-4-fluoromethylbenzoyl)-1,3-cyclohexanedione) and mesotrione, inhibitors of 4-hydroxyphenyl pyruvate dioxygenase (HPPD) following a single dose to healthy male volunteers, *Br. J. Clin. Pharmacol. 52*, 169−177.
39. Romagni, J. G., Meazza, G., Nanayakkara, N. P., and Dayan, F. E. (2000) The phytotoxic lichen metabolite, usnic acid, is a potent inhibitor of plant *p*-hydroxyphenylpyruvate dioxygenase, *FEBS Lett. 480*, 301−305.
40. Ellis, M. K., Whitfield, A. C., Gowans, L. A., Auton, T. R., Provan, W. M., Lock, E. A., and Smith, L. L. (1995) Inhibition of 4-hydroxyphenylpyruvate dioxygenase by 2-(2-nitro-4- trifluoromethylbenzoyl)-cyclohexane-1,3-dione and 2-(2-chloro-4- methanesulfonylbenzoyl)-cyclohexane-1,3-dione, *Toxicol. Appl. Pharmacol. 133*, 12−19.
41. Laskowski, R. A., Macarthur, M. W., Moss, D. S., and Thornton, J. M. (1993) Procheck−A Program to Check the Stereochemical Quality of Protein Structures, *J. Appl. Crystallogr. 26*, 283−291.
42. Engh, R. A., and Huber, R. (1991) Accurate bond and angle parameters for X-ray protein structure refinement, *Acta Crystallogr., Sect. A 47*, 392−400.

BI049317S